LARGE-SCALE THERMAL-SHOCK EXPERIMENTS WITH CLAD AND UNCLAD STEEL CYLINDERS*

R. D. Cheverton
Oak Ridge National Laboratory
Oak Ridge, Tennessee

Abstract

Flaw behavior trends associated with pressurized-thermal-shock (PTS) loading of pressurized-water-reactor pressure vessels have been under investigation at the Oak Ridge National Laboratory for nearly 20 years. During that time, twelve thermal-shock experiments with thick-walled (152 mm) steel cylinders were conducted as a part of the investigations. The first eight experiments were conducted with unclad cylinders initially containing shallow (8–19 mm) two-dimensional and semicircular inner-surface flaws. These experiments demonstrated, in good agreement with linear elastic fracture mechanics, crack initiation and arrest, a series of initiation/arrest events with deep penetration of the wall, long crack jumps, arrest with the stress intensity factor (K_I) increasing with crack depth, extensive surface extension of an initially short and shallow (semicircular) flaw, and warm prestressing with $\dot{K}_I \leq 0$.

The remaining four experiments were conducted with clad cylinders containing initially shallow (19–24 mm) semielliptical subclad and surface flaws at the inner surface. In the first of these experiments one of six equally spaced (60°) "identical" subclad flaws extended nearly the length of the cylinder (1220 mm) beneath the cladding (no crack extension into the cladding) and nearly 50% of the wall, radially. For the final experiment, four of the semielliptical subclad flaws that had not propagated previously were converted to surface flaws, and they experienced extensive extension beneath the cladding with no cracking of the cladding.

Information from this series of thermal-shock experiments is being used in the evaluation of the PTS issue.

DISCLAIMER

*Research sponsored by the Office of Nuclear Regulatory Research, U.S. Nuclear Regulatory Commission under Interagency Agreement 1886-8011-9B with the U.S. Department of Energy under Contract DE-AC05-84OR21400 with Martin Marietta Energy Systems, Inc.

THERMAL-SHOCK EXPERIMENTS WITH LARGE, CLAD AND UNCLAD TEST CYLINDERS

1. INTRODUCTION

The pressurized thermal shock (PTS) issue pertaining to pressurized water reactors (PWRs) has been under intensive investigation by the Nuclear Regulatory Commission (NRC), reactor vendors, and utilities since the early 1970s, and these efforts resulted in issuance, by the NRC, of the PTS Rule[1] and Regulatory Guide 1.154 (Ref. 2). As an aid in formulating the rule and Regulatory Guide, the NRC sponsored the Integrated Pressurized Thermal Shock (IPTS) Program, which involved development of probabilistic models and the subsequent calculation of the frequency of vessel failure for three specific plants.[3–5] The validity of the deterministic aspects of the probabilistic fracture mechanics model included in the IPTS methodology was established to a large extent on the basis of a series of thermal-shock experiments conducted with thick-walled steel cylinders.[6] These experiments were conducted without cladding, which normally exists on the inner surface of PWR pressure vessels and presumably influences the behavior of flaws in the proximity of the cladding. An "acceptable" method for including cladding in the IPTS studies was to account for its relatively low thermal conductivity in the thermal analysis and its relatively high coefficient of thermal expansion in the stress analysis, and to assume that initial flaws penetrated the cladding (surface flaws) and that the cladding had the same fracture toughness properties, including irradiation effects, as the base material. More recently, there has been a desire to obtain a better understanding of the role of cladding. To address this need, "typical" cladding material has been irradiated,[7] clad-plate[8,9] and clad-beam[10] tests with mechanical loading have been conducted, and thermal-shock experiments, similar to the earlier ones, but with cladding on the inner surface, have been conducted.[11]

There has also been a growing interest in the effect of constraint on fracture toughness for PTS-related conditions. The IPTS studies indicated that most flaws resulting in calculated failures were very shallow (crack depth <15 mm), and beam experiments[12] indicate that such flaws may have elevated toughness (relative to plane-strain values) associated with them (attributed to reduced constraint). Yet, there is some concern that out-of-plane tensile stress, a relatively high yield stress, and/or a steep gradient in stress[13,14] could, at least to some extent, negate the elevation. The thermal-shock experiments tend to address these phenomena because shallow flaws, steep stress gradients, a relatively high yield stress, and a biaxial stress state are involved.

Another area of recent interest pertains to the possible existence and effects of low-toughness sites, which, in principle, could result in a structure effective crack-initiation fracture toughness as low as the crack arrest toughness of the material surrounding the low-toughness site.[15] The thermal-shock experiments tend to address this subject because of the extensive length of crack front involved, which increases the chances of a low-toughness site existing. However, no welds, other than the cladding (weld deposition), were included in the test cylinders, and it may be that low-toughness sites are more likely to exist in welds than base material.

The purpose of this paper is to review and compare the thermal-shock experiments with and without cladding, particularly in light of present interests in flaw-depth, stress-gradient, yield-stress, and stress-state effects on effective fracture toughness and the concern over low-toughness sites. Detailed analyses of the experiments are still being conducted, and thus this paper does not represent a final evaluation. Presumably there is more to be learned from these experiments as our insights and analytical tools are improved.

2. OBJECTIVES OF THERMAL-SHOCK EXPERIMENTS

As indicated in Figs. 1 and 2 and discussed in Ref. 11, a linear elastic fracture mechanics (LEFM) analysis of a PWR vessel subjected to PTS loading indicates (1) essentially a biaxial stress state; (2) steep gradients in temperature, stress, stress intensity factor (K_I) and critical values of K_I corresponding to initiation (incipient propagation) (K_{Ic}) and arrest (K_{Ia}); (3) a series of initiation and arrest events; (4) initiation of very shallow flaws; (5) arrest with K_I increasing with increasing crack depth (in a standard crack-arrest test K_I decreases with increasing crack depth); (6) warm prestressing (WPS) with $K_I < 0$; (7) the possibility of long crack jumps that might introduce dynamic effects; and (8) at least in the absence of cladding a short surface crack could extend on the surface to become a long flaw with an increased potential for propagating radially. These indicated events and features raised questions about the applicability of lab-specimen K_{Ic} and K_{Ia} data for PTS analyses (constraint effects associated with shallow flaws and steep stress gradients; arrested crack fronts; arrest with $dK_I/da > 0$) and about whether warm prestressing, dynamic events, and extensive surface extension would take place under PTS conditions. Obtaining answers to these questions was a major part of the objective of the thermal-shock program.

The objective also included, of course, a determination of the behavior of flaws in the presence of cladding. By comparison with an unclad vessel, the presence of cladding (1) reduces the severity of the PTS thermal shock (relatively low thermal conductivity) and thus tends to reduce the potential for propagation of flaws; and (2) introduces high thermal stresses near the surface (relatively high coefficient of thermal expansion) and thus tends to increase the potential for propagation of surface flaws. As suggested in Refs. 16–18, the cladding provides a crack-mouth closing force for subclad flaws (Fig. 3) that reduces K_I relative to that for a surface flaw. The crack-mouth closing force is essentially equal to the stress in the cladding times the thickness of the cladding, and for severe thermal-shock loading conditions this stress is the "yield" stress. The possible benefit of cladding for a subclad flaw, relative to a surface flaw and in terms of reducing K_I for the portion of the crack front in the base material, is dependent on the extent of stretching of the cladding over the crack. As the stretching increases, the benefit decreases. Because of complexities associated with modeling of the crack tip at the clad/base interface, the accuracy of the calculated extent of stretching is quite uncertain. Thus, an experimental determination is necessary and was included in the scope of the thermal-shock experiments with a clad cylinder.[11]

Another cladding-related phenomenon that is difficult to model at the present time is the tendency for either a surface or subclad flaw to propagate beneath the cladding. If subclad propagation (tunneling) is restricted, limiting the length of the flaw, the potential for radial propagation will be less.

3. DESCRIPTION OF EXPERIMENTS

3.1 Test Cylinders

Nine thermal-shock experiments (TSE-4, 5, 5A, 6–11) are discussed in this paper. Each was conducted with a test cylinder fabricated from A508 steel with class-2 chemistry. Three different heat treatments were used, the difference being in the tempering temperature following quenching in water from the austenitizing temperature (860°C). At the time of quenching, the cylinders were oversize so that final machining would preclude significant residual stresses. The length of the cylinders was sufficient to eliminate significant end effects in the central portion of the cylinder. New, unclad, test cylinders were used for each of the first five experiments (TSE-4, 5, 5A, 6, and 7), and one additional cylinder, clad on the inner surface, was used for TSE-8, 9, 10, and 11. Two cladding materials were used for the clad cylinder (Fig. 4), and both were applied by the strip-cladding, submerged-arc process. Stainless steel 304L was applied to a 90° segment, while the remaining 270° was clad with Inconel 600. All test cylinders but the one for TSE-4 were

the same in length and outside diameter. The test cylinder for TSE-4 was smaller and had a small enough ratio of diameter to wall thickness to preclude deep penetration of the flaw. A summary of descriptive material is provided in Table 1, and more detail is given in Refs. 6, 11, 19, 20, and 21. Photographs of a clad and unclad test cylinder are shown in Figs. 5 and 6.

Table 1. Summary of test conditions for ORNL thermal shock experiments

Parameter	Experiment					
	TSE-4	TSE-5	TSE-5A	TSE-6	TSE-7	TSE-8,9,10,11
Cylinder dimensions, mm						
Outside diameter	533	991	991	991	991	991
Wall thickness	152	152	152	76	152	152
Length	914	1220	1220	1220	1220	1220
Cladding thickness						5.6
Cylinder material						
Designation			A508, Class 2 chemistry			
Tempering temperature, °C	AQ[a]	613	679	613	704	620
RT_{NDT}, °C	75	66	10	66	−1	66
Yield stress at 22°C, MPa	900	682	581	682	449	520
Flaw (initial)						
Type	LS[b]	LS, SS[c]	LS	LS	SCS[d]	SES,[e] SESC[f]
Orientation	axial	axial, circum.	axial	axial	axial	axial
Length, mm	914	1220, 10	1220	1220	37	114, 38 (Fig. 7
Depth, mm	11	16	11	7.6	14	19)
Thermal shock						
Initial temperature of cylinder, °C	288	96	96	96	96	96
Initial temperature of coolant, °C	−25	−196	−196	−196	−196	−196
Quench medium	W/A[g]	LN_2[h]	LN_2	LN_2	LN_2	LN_2

[a]AQ = as quenched.
[b]LS = long, surface.
[c]SS = short, surface
[d]SCS = semicircular, surface.
[e]SES = semielliptical, surface.
[f]SESC = semielliptical, subclad.
[g]W/A = water/alcohol.
[h]LN_2 = liquid nitrogen.

3.2 Flaws

Initial flaws for the experiments were "shallow" (≤19 mm) and were generated with the electron-beam, hydrogen-charge technique,[22] which results in a sharp, arrested crack for the initial flaw. All intended flaws were oriented in an axial direction. For experiments TSE-4, 5, 5A, and 6, the intended initial flaws were surface cracks that extended the length of the test cylinder with uniform depth. The flaw for TSE-7 was a semicircular surface crack. The test cylinder used for TSE-8, 9, 10, and 11 had multiple flaws with arrestor holes in close proximity in an attempt to control interaction effects after flaw extension. As indicated in Figs. 4 and 7, there were six,

equally spaced (60°), 6/1 semielliptical, subclad flaws for TSE-8. Following TSE-8, two semicircular surface flaws were added, and following TSE-10 four of the subclad flaws in the Inconel-clad area were converted to surface flaws by slitting the cladding; these latter flaws had not propagated previously.

3.3 Experiment Technique

To simulate radiation embrittlement and otherwise provide appropriate conditions for propagation of flaws, it was necessary to use a low-temperature thermal-shock medium and, for some experiments, a low-tempering temperature (both of which contributed to low-fracture toughness) and a severe thermal shock (high stress intensity factors). This is not surprising when we recall that flaw propagation in PWR vessels is predicted only when considering high fluences, high copper and nickel concentrations, lower-bound fracture toughness, and severe transients.

The desired thermal-shock conditions were achieved for TSE-4 by heating the test cylinder to 288°C and quenching the inner surface with an alcohol/water mixture at –25°C. For all successive experiments the test cylinder was heated to 96°C and quenched with liquid nitrogen (–196°C). For the latter experiments, the ends and outer surface of the test cylinder were thermally insulated. After heating, and with all instrumentation attached, the test cylinder assembly was lowered into a tank of liquid nitrogen. (A special surface coating was used to promote nucleate boiling, which provided the necessary high heat transfer coefficient.) The thermal shock was delayed, until full submergence of the test cylinder, by a gas bubble, trapped in the cavity, that was released after complete submergence was achieved. This procedure resulted in a very uniform thermal shock to the inner surface.

Instrumentation included 15 thermocouple thimbles with 12 thermocouples each for measuring the temperature distribution in the wall during a transient; weldable strain gages, as crack-opening-displacement gages, for detecting the times of initiation/arrest events, and, indirectly, for determining crack depth; and ultrasonic instrumentation for detecting time of events and crack depth.

After the final experiment with a specific test cylinder, the flawed region was removed and the fracture completed, by mechanical means, at liquid-nitrogen temperature to reveal the fracture surfaces. In some cases, examination of the fracture surfaces was aided by scanning electron microscopy.

3.4 Specific Purpose of Each Experiment

Generic: to demonstrate that linear elastic fracture mechanics (LEFM) is valid for application to PTS loading. One way of doing this is to compare the thermal-shock-experiment critical values of K_I corresponding to the initiation and arrest events with K_{Ic} and K_{Ia} data measured with standard specimens. This could be an oversimplification, however, if, for instance, out-of-plane stress, a relatively high yield stress, and/or very steep stress gradients, all of which were characteristic of the specific thermal-shock experiments,[6] nullified lack-of-constraint enhancement of fracture toughness associated with the shallow flaws tested under uniaxial, shallow-gradient-stress conditions.[12]

TSE-4: to demonstrate initiation and arrest. It was not anticipated that more than one initiation/arrest event would take place because of the stiffness of the wall (low ratio of radius to wall thickness).

TSE-5: to demonstrate a series of initiation/arrest events with deep penetration of the wall and with warm prestressing limiting the number of events.

TSE-5A: the same as that for TSE-5, with the addition of arrest with $dK_I/da > 0$. The fracture toughness was purposely greater than for TSE-5 (RT_{NDT} = 10°C for TSE-5A compared to 66°C for TSE-5).

TSE-6: to demonstrate that as a result of a very long crack jump, dynamic effects would not be large enough to drive the flaw completely through the wall. A thinner wall (higher radius-to-wall-thickness ratio) was required to achieve the long crack jump.

TSE-7: to demonstrate that in the absence of cladding an initially short surface flaw would extend on the surface in a single event to become a long flaw.

TSE-8: to evaluate the behavior of subclad flaws.

TSE-9: to evaluate the behavior of shallow, semicircular, surface flaws in the presence of cladding. The intent was to terminate the experiment after the first event so that the fracture contour associated with the first event could be determined. (The occurrence of a subsequent event might prevent that determination.)

TSE-10: to evaluate the behavior of shallow, semicircular, surface flaws in the presence of cladding. As opposed to TSE-9, the duration of the transient was to be sufficient for all possible events to take place.

TSE-11: to evaluate the behavior of shallow, 6/1 semielliptical, surface flaws in the presence of cladding.

4. RESULTS AND DISCUSSION

4.1 Temperature Transients

The temperature transients achieved (Figs. 8 and 9) were such that within 2 min the inner-surface temperatures dropped 270°C for TSE-4 and 170–240°C for the subsequent experiments. The rather large variation for the latter experiments was not intentional but was due in part to unintended variations in the surface coating that must be used to enhance the fluid-film heat transfer coefficient. The initial rate of decrease in surface temperature was greater for the clad test cylinder because of the insulating effect of the cladding, and was greater yet for TSE-4 because of forced-convection cooling. In all cases, the initial difference in temperature between test cylinder and quench medium was about the same (~300°C).

4.2 Fracture Behavior

The evaluation of the actual flaw behavior involves a calculation of K_I, K_{Ic}, and K_{Ia}. To minimize uncertainties, these parameters were calculated using the measured temperature distributions. Also, some fracture-toughness data were obtained specifically for the test-cylinder materials, and these data were used in conjunction with an existing data base[23] to obtain best-estimate values. LEFM two- and three-dimensional (2-D and 3-D) finite-element models were used for calculating K_I values for TSE-4, 5, 5A, 6, and 7, but for TSE-8, 9, 10, and 11 elastic-plastic fracture mechanics (EPFM) models were used to account for the large amount of plasticity in the cladding. Values of K_I/K_{Ic} mentioned below are consistent with this approach.

4.2.1 TSE-4

During TSE-4 there was one initiation/arrest event (Figs. 10 and 11). It took place at 152 s into the transient, and the best-estimate value of K_I/K_{Ic} at the time of initiation was 1.06. A second initiation event was prevented by WPS. The flaw extended 10 mm and arrested with $dK_I/da \equiv 0$. As indicated by the set of critical crack depth curves (Fig. 11),* there is reasonably good agreement between predicted (using actual temperatures) and actual flaw behavior.

---

* A set of critical-crack-depth curves consists of a plot of crack depths corresponding to initiation and arrest events and incipient WPS ($K_I = 0$), all as a function of time in the transient.

4.2.2 TSE-5

During TSE-5 there were three initiation/arrest events associated with the intended long, axial flaw, and WPS prevented a fourth event (Figs. 12 and 13). As indicated in Fig. 13, the second event was delayed, indicating an elevated toughness and thus resulting in a rather long crack jump. The long jump introduced the possibility of dynamic effects, but the good agreement between calculated (static analysis) and actual arrested crack depth indicates dynamic effects were not significant.

An unintended and initially undetected surface flaw with a surface length of only 10 mm, a depth of 16 mm, and a circumferential orientation (a cross crack in the EB-weld fusion zone used to generate the long axial flaw) extended on the surface, bifurcating many times, to become a very long flaw (Fig. 14). This confirmed a predicted behavior that was to be investigated in a later experiment (TSE-7). Propagation of this flaw occurred after propagation of the long axial flaw and thus did not influence propagation of the latter flaw.

4.2.3 TSE-5A

During TSE-5A there were four initiation/arrest events with WPS preventing a fifth event (Fig. 15). Following incipient WPS ($\dot{K}_I = 0$), K_I/K_{Ic} reached a maximum value of 2.3, and yet initiation did not take place. Thus, WPS (no initiation with $\dot{K}_I < 0$) was demonstrated in a reasonably convincing manner, and once again there was good agreement between prediction and experiment.

4.2.4 TSE-6

During TSE-6 there were two initiation/arrest events with a final arrest 95% of the way through the wall (Figs. 16 and 17). The static LEFM analysis predicted the deep arrest, but there was concern that dynamic effects might drive the flaw completely through the wall. Apparently, dynamic effects were negligible.

4.2.5 Comparison of fracture-toughness data from TSE-4, 5, 5A, and 6

A comparison of standard-specimen K_{Ic} and K_{Ia} data* with the critical K_I values corresponding to the initiation and arrest events detected during the ORNL thermal-shock experiments and a similar French experiment[24] (Figs. 18 and 19) shows good agreement and thus indicates that LEFM is valid for PTS loading, assuming that the shallow initial flaws would not exhibit a substantially elevated toughness. Shallow-flaw data obtained with beams subjected to bending[12] indicate that the first initiation events for TSE-5 and TSE-6 were at too low a temperature to exhibit elevated toughness; however, for TSE-4, TSE-5A and the French experiment, they were not. Even so, there is no evidence in Fig. 18 of elevated toughness. A possible explanation is that out-of-plane stresses (nearly equal biaxial stresses under thermal-shock loading), and/or the relatively high yield stress,** and/or the steep gradient in stress over the depth of the flaw resulted in a reduction in fracture toughness based on the single fracture parameter K_I (Refs. 13 and 14). This possibility is under investigation at ORNL.

---

*The data used for the comparison discussed herein are those used to define the ASME lower-bound K_{Ic} and K_{Ia} curves.[23]

**The room-temperature yield stress for the shallow-flaw beams was ~420 MPa, which is low compared to the values for the test cylinders (Table 1).

The two relatively high data points in Fig. 18 correspond to the initiation events that preceded the two long crack jumps (TSE-5 and TSE-6), and in Fig. 19 it is not evident that the long crack jumps had a significant effect on crack arrest (data points are within the scatter band).

Two other data points of particular interest in Fig. 19 are those corresponding to arrest with $dK_I/da > 0$. There is not a discernible difference between these data points and data obtained from a standard crack-arrest test ($dK_I/da < 0$). Thus, the latter data appear to be valid for PTS loading.

During TSE-5, 5A, 6, and 7, there were more than 12 initiation events involving crack fronts totaling more than 1000 mm in length, and yet the existence of low-toughness sites is not apparent; that is, K_{Ic} values deduced from the experiments do not fall below the ASME lower-bound K_{Ic} curve. On the other hand, there is considerable overlap of the K_{Ic} and K_{Ia} scatterbands, which implies that the lower part of the K_{Ic} scatterband includes the effect of low-toughness sites.[15] This is consistent with the notion that if a compact specimen containing a low-toughness site fails, as opposed to exhibiting a pop-in, the existence of the low-toughness site results in a relatively low value of K_{Ic} but otherwise is not recognized. A pop-in eliminates the low-toughness site without failure and presumably is not recorded as a K_{Ic} value. Thus, perhaps the ASME lower-bound K_{Ic} curve includes essentially all low-toughness sites that can result in failures.

4.2.6 TSE-7

During TSE-7, the shallow, semicircular flaw experienced three major initiation/arrest events and, during the first event, extended on the surface, bifurcating many times, to become a very long flaw (Fig. 20). The pretest analysis, which could not include the potential for bifurcation, indicated that the flaw would extend on the surface nearly the full length of the test cylinder in a single event and subsequently experience two more initiation/arrest events with a fourth event being prevented by WPS (Fig. 21). (The 2-D analysis presented in Fig. 21 is reasonably accurate because the maximum value of K_I/K_{Ic} for the semicircular and 2-D flaws of the same depth are about the same, and the first event extends the surface length of the initial flaw.) Thus, there was good agreement between prediction and experiment.

4.2.7 TSE-8

During TSE-8, one of the six flaws (flaw 3) experienced two initiation/arrest events, extending both the length and depth of the flaw (Fig. 22). Although there were obvious stretch marks in the cladding over the extended flaw, there was no penetration of the cladding. The maximum value of K_I/K_{Ic} along the original crack front at the time of the initial initiation was at the deepest point and was 0.8. The maximum values achieved for the other five flaws occurred somewhat later and were nominally 1.0 (as a result of the extensive extension of flaw 3, there was a loss of symmetry that increased K_I slightly for some flaws and decreased K_I slightly for others). This experiment demonstrated that even in the presence of tough cladding, a short flaw could extend in length beneath the cladding to effectively become a 2-D subclad flaw. Comparing TSE-8 with TSE-7 indicates that the presence of the cladding reduces the tendency for bifurcation and thus the extent of "surface" extension.

The calculation of K_I for the portion of the crack front in the base material required modeling of the crack front at the clad/base interface, and this was done using a crack-tip blunting model.[11] The low calculated value of K_I/K_{Ic} for the first event (0.8) indicates that stretching of the cladding over the flaw was greater than calculated.

4.2.8 TSE-9 and TSE-10

TSE-9 and TSE-10 included two semicircular surface flaws, one of which extended slightly during TSE-9. Immediately following this event, which was nothing more than completion of crack generation in the EB-weld fusion zone, the transient was terminated by withdrawing

the test cylinder from the liquid nitrogen. Although of greater duration, the thermal transient for TSE-10 was less severe (Fig. 9), and there was no further propagation. The maximum value of K_I/K_{Ic} during TSE-9 for the portion of the crack front in the base material occurred at the clad/base interface and was 1.3. This value, however, is based on the toughness of the base material in essentially a quench-only condition, and it may be that the heat affected zone at the clad/base interface was tempered to a higher toughness. In any case, because the TSE-7 test cylinder was fully temperated ($RT_{NDT} = -1°C$), and because the TSE-9 transient was somewhat more severe (Figs. 8 and 9), it appears that the presence of cladding reduced the potential for propagation of the semicircular surface flaw. This is further supported by the lack of propagation during TSE-11, which had a more severe transient.

4.2.9 TSE-11

The thermal transient for TSE-11 was substantially more severe than those for the other experiments (Fig. 9). During the transient, the four 6/1, semielliptical, surface flaws propagated, extending in length and depth without penetrating the cladding (Fig. 23 and Table 2). There was some bifurcation that permitted flaw 6 to bypass the arrestor holes and extend nearly to the ends of the cylinder. There is evidence in Table 2 that at 124 and 230 s initiation of one flaw triggered others, presumably as a result of stress waves. Values of K_I/K_{Ic} at the times of the first initiations were 1.1 (clad/base interface) and 0.8 (deepest point) at 86 s and 1.3 (clad/base interface) and 1.1 (deepest point) at 124 s, all based on $RT_{NDT} = 66°C$. The extension of flaw 2 at 86 s was restricted, as intended, by arrestor holes and thus had a negligible effect on the events associated with the other flaws at 124 s.

Table 2. Events during TSE-11

Flaw	Time (s)				
	86	124	192	230	390
2	E[a]	E			
3		E	E	E	E
4		E			
5		E			
6		E		E	

[a]E indicates initiation/arrest events.

Flaw 3, which had propagated during TSE-8, experienced four additional initiation/arrest events, while the subclad flaw in the stainless-steel-clad region (flaw 1) and the two semicircular surface flaws (flaws 7 and 8) did not propagate. The maximum value of K_I/K_{Ic} for flaw 1 prior to WPS (~230 s) and prior to extensive propagation of other flaws (124 s) was 1.0, and it was at the deepest point. For the semicircular flaws, the corresponding value was 1.5 at the clad base interface (based on $RT_{NDT} = 66°C$) and 0.8 at the deepest point.

5. SUMMARY

The thermal-shock experiments confirmed the validity of LEFM for severe thermal-shock loading conditions by demonstrating the following flaw behavior trends in good agreement with analysis:

a. initiation of very shallow flaws;
b. arrest of both short- and long-crack jumps;
c. a series of initiation/arrest events with deep penetration of the wall;
d. the inability of a flaw to initiate with $\dot{K}_I < 0$, even though $K_I/K_{Ic} >> 1.0$ (Type-1 WPS);
e. arrest with $dK_I/da > 0$;
f. extensive surface extension in a single event and in the absence of cladding of an initially short and shallow surface flaw; and
g. extensive subclad extension at the clad/base interface of an initially short and shallow surface or subclad flaw, although the analytical model for subclad propagation is suspect because of geometric complexities.

The validity of LEFM is illustrated in a quantitative sense by the good agreement between critical values of K_I, corresponding to initiation and arrest events, and K_{Ic} and K_{Ia} values measured with standard procedures. The good agreement in K_{Ia} values for a long crack jump should not, however, be interpreted to mean that dynamic effects are necessarily negligible for PWR pressure vessels, which have higher ratios of vessel radius to wall thickness.[25,26] Also, the good agreement of K_{Ic} values should not be interpreted to mean that constraint effects associated with shallow flaws will not be significant under more nearly typical PWR PTS conditions. This issue is presently under investigation at ORNL.

There was no evidence of low-toughness sites other than the observation that some of the K_{Ic} values deduced from the thermal shock experiments approached the ASME lower-bound K_{Ic} curve.

6. REFERENCES

1. "Fracture Toughness Requirements for Protection Against Pressurized Thermal Shock Events," *Federal Register*, Vol. 50, No. 141, Section 50.61, pp. 29937–29945 (July 23, 1985).

2. *Regulatory Guide 1.154*, "Format and Content of Plant-Specific Pressurized Thermal Shock Safety Analysis Reports for Pressurized Water Reactors," U.S. Nuclear Regulatory Commission, Office of Nuclear Regulatory Research, January 1987

3. T. J. Burns et al., *Pressurized Thermal Shock Evaluation of the Oconee-1 Nuclear Power Plant*, NUREG/CR-3770 (ORNL/TM-9176), Martin Marietta Energy Systems, Inc., Oak Ridge National Laboratory, May 1986.

4. D. L. Selby et al., *Pressurized Thermal Shock Evaluation of the Calvert Cliffs Unit 1 Nuclear Power Plant*, NUREG/CR-4022 (ORNL/TM-9408), Martin Marietta Energy Systems, Inc., Oak Ridge National Laboratory, September 1985.

5. D. L. Selby et al., *Pressurized Thermal Shock Evaluation of the H. B. Robinson Unit 2 Nuclear Power Plant*, NUREG/CR-4183 (ORNL/TM-9567), Vols. 1 and 2, Martin Marietta Energy Systems, Inc., Oak Ridge National Laboratory, September 1985.

6. R. D. Cheverton, S. K. Iskander, and D. G. Ball, "Review of Pressurized-Water-Reactor-Related Thermal-Shock Studies," pp. 752–766 in *Fracture Mechanics: Nineteenth Symposium*, ASTM STP 969, T. A. Cruse, Ed., American Society for Testing and Materials, Philadelphia, 1988.

7. W. R. Corwin et al., "Fracture Behavior of a Neutron-Irradiated Stainless Steel Submerged Arc Weld Cladding Overlay," *Nucl. Engrg. Des.*, 89, pp. 199–221 (1985).

8. W. R. Corwin, "Reactor Vessel Cladding Separate Effects Studies," *Nucl. Engrg. Des.*, 98, pp. 171–193 (1987).

9. S. K. Iskander et al., *Experimental Results of Tests to Investigate Flaw Behavior of Mechanically Loaded Stainless Steel Clad Plates*, NUREG/CR-5785 (ORNL/TM-11950), Martin Marietta Energy Systems, Inc., Oak Ridge National Laboratory, April 1992.

10. D. E. McCabe, *Fracture Evaluation of Surface Cracks Embedded in Reactor Vessel Cladding*, NUREG/CR-4841 (MEA-2200), Materials Engineering Associates, Inc., May 1987.

11. R. D. Cheverton et al., "Thermal Shock Experiments with Flawed Clad Cylinders," *Nucl. Engrg Des.*, 124, pp. 109–119 (1990).

12. T. J. Theiss, D. K. M. Shum, and S. T. Rolfe, *Experimental and Analytical Investigation of the Shallow-Flaw Effect in Reactor Pressure Vessels*, NUREG/CR-5886 (ORNL/TM-12115), Martin Marietta Energy Systems, Inc., Oak Ridge National Laboratory, July 1992.

13. W. E. Pennell, "Aging Impact on the Safety and Operability of Nuclear Reactor Pressure Vessels," in *Proceedings of the Aging Research Information Conference*, Holiday Inn Crowne Plaza, Rockville, Maryland, March 24–27, 1992, NUREG/CP-0122, Vol. 1.

14. D. K. M. Shum and B. R. Bass, *Absence of Toughness Elevation in Thermal-Shock Experiment TSE-5A: Preliminary Explanation Based on Crack-Tip Constraint*, ORNL/NRC/LTR-92/24, October 1992.

15. R. D. Cheverton and S. K. Iskander, "Thermal Shock Investigations" pp. 87–93 in *Heavy-Section Steel Technology Program Quarterly Progress Report for January–March 1981*, NUREG/CR-2141/V1 (ORNL/TM-8722), Martin Marietta Energy Systems, Inc., Oak Ridge National Laboratory, June 1981.

16. R. D. Cheverton et al., *Heavy Section Steel Technology Program Quarterly Progress Report for July–September 1981*, NUREG/CR-2141, Vol. 3 (ORNL/TM-8145), pp. 91-93, February 1982.

17. E. Smith, "The Effect of Austenitic Cladding on the Extension of an Under-Clad Crack into the Wall of a Water-Cooled Nuclear Reactor Pressure Vessel During a Hypothetical Loss of Coolant Accident," *Trans. 7th Int. Conf. on Structural Mechanics in Reactor Technology*, Vol. G, pp. 143–148, August 1983.

18. E. Smith, "The Restraining Effect of Austenitic Cladding on the Extension of a Three-Dimensional Crack into the Wall of a Water-Cooled Nuclear Reactor Pressure Vessel During a Hypothetical Overcooling Accident," *Nucl. Engrg. Des.*, 78, pp. 79–84 (1984).

19. R. D. Cheverton and S. E. Bolt, *Pressure Vessel Fracture Studies Pertaining to a PWR LOCA-ECC Thermal Shock: Experiments TSE-3 and TSE-4 and Update of TSE-1 and TSE-2 Analysis*, ORNL/NUREG-22, Marietta Energy Systems, Inc., Oak Ridge National Laboratory, December 1977.

20. R. D. Cheverton et al., *Pressure Vessel Fracture Studies Pertaining to the PWR Thermal-Shock Issue: Experiments TSE-5, TSE-5A, and TSE-6*, NUREG/CR-4249 (ORNL-6163), Marietta Energy Systems, Inc., Oak Ridge National Laboratory, June 1985.

21. R. D. Cheverton et al., *Pressure Vessel Fracture Studies Pertaining to the PWR Thermal-Shock Issue: Experiment TSE-7*, NUREG/CR-4304 (ORNL-6177), Marietta Energy Systems, Inc., Oak Ridge National Laboratory, August 1985.

22. P. P. Holz, "Preparation of Long Axial Flaw for TSE-5A," pp. 35–37 in *Heavy-Section Steel Technology Program Quarterly Progress Report July–September 1980*, NUREG/CR-1806 (ORNL/NUREG/TM-419), Marietta Energy Systems, Inc., Oak Ridge National Laboratory, December 1980.

23. *Flaw Evaluation Procedures – Background and Application of ASME Section XI, Appendix A, NP-719-SR*, Prepared by American Society of Mechanical Engineers, Section XI Task Group on Flaw Evaluation, T. U. Marson, Ed., Special Report, August 1978.

24. A. Pellissier-Tanon, P. Sollogoub, and B. Houssin, "Crack Initiation and Arrest in an SA 508 Class-3 Cylinder Under Liquid Nitrogen Thermal-Shock Experiment," *Transactions of the 7th International Conference on Structural Mechanics in Reactor Technology*, Vols. G and H., North Holland Publishing Co., Amsterdam, The Netherlands, August 1983.

25. J. Keeney-Walker and B. R. Bass, *A Comparison of Analysis Methodologies for Predicting Cleavage Arrest of a Deep Crack in a Reactor Pressure Vessel Subjected to Pressurized-Thermal-Shock Loading Conditions*, NUREG/CR-5793 (ORNL/TM-11969), Marietta Energy Systems, Inc., Oak Ridge National Laboratory, September 1992.

26. D. J. Ayres et al., *Tests and Analyses of Crack Arrest in Reactor Vessel Materials*, Final Report, NP-5121M on EPRI Research Project 2180-3, April 1987.

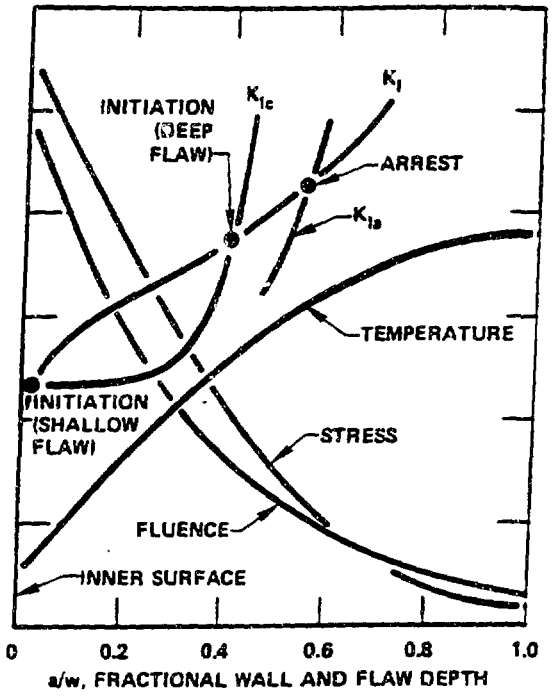

Fig. 1. Fracture parameters vs flaw depth and radial position in wall at specific time in severe PTS transient (high copper, nickel, and fluence).

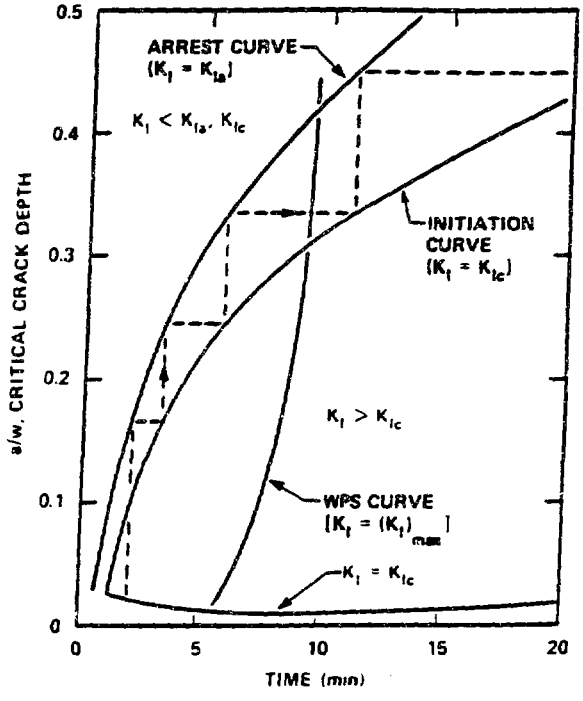

Fig. 2. Critical-crack-depth curves for severe PTS transient (high copper, nickel, and fluence).

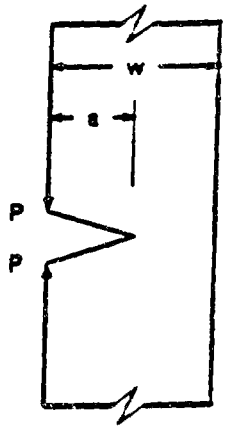

Fig. 3. Crack-mouth closing force associated with tensile stress in cladding over subclad flaw.

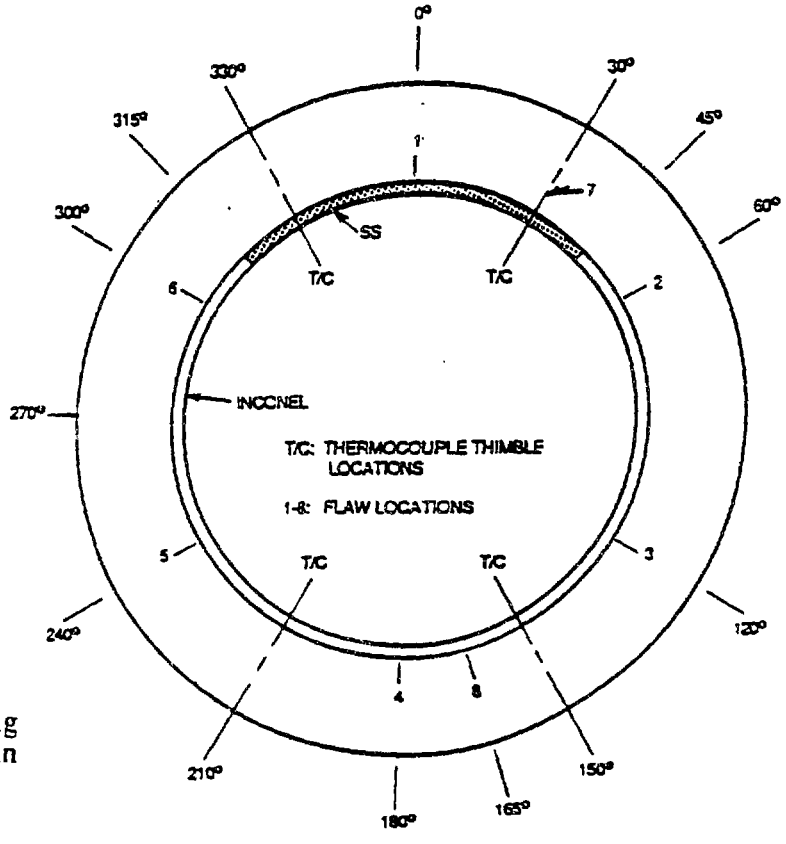

Fig. 4. Cladding configuration and flaw locations in test cylinder for TSE-8, 9, 10, and 11.

Fig. 5. Typical test cylinder used for TSE-5, 5A, 6, 7 (no cladding).

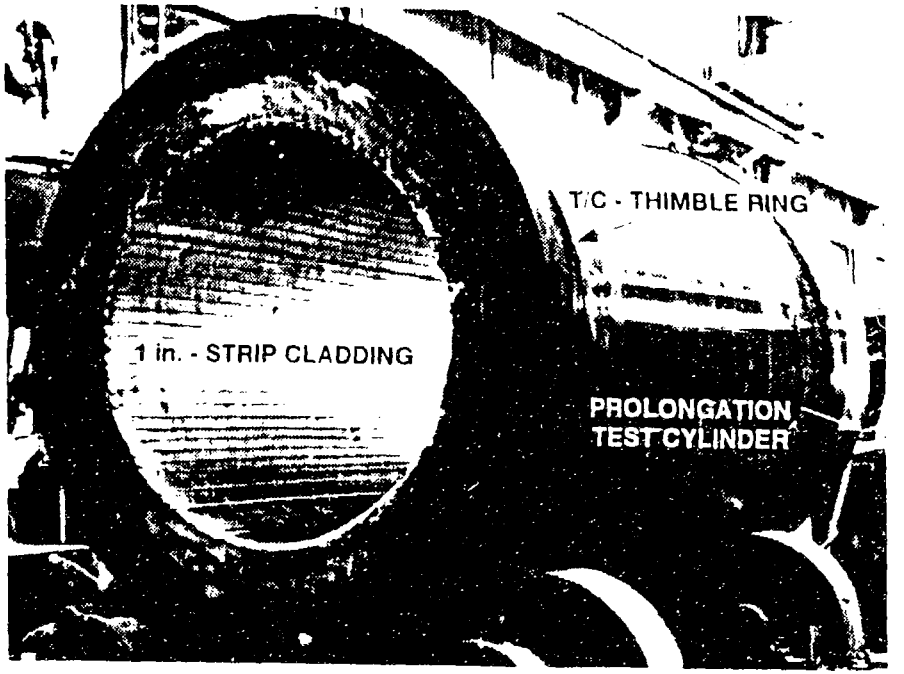

Fig. 6. Test-cylinder/prolongation assembly showing strip cladding before machining.

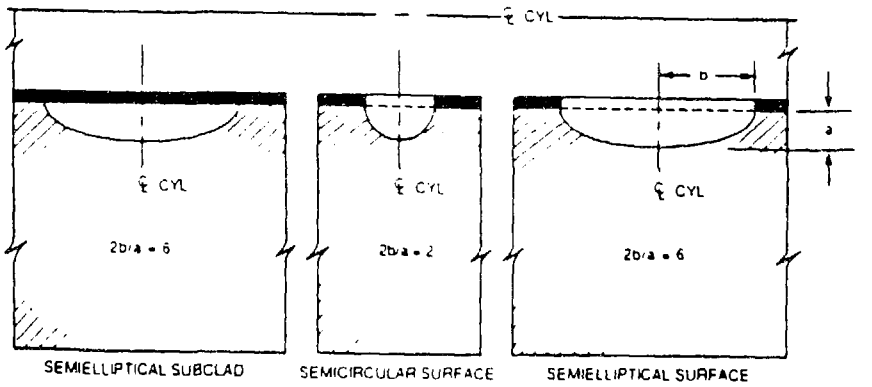

Fig. 7. Types of flaws for the clad-cylinder series of experiments.

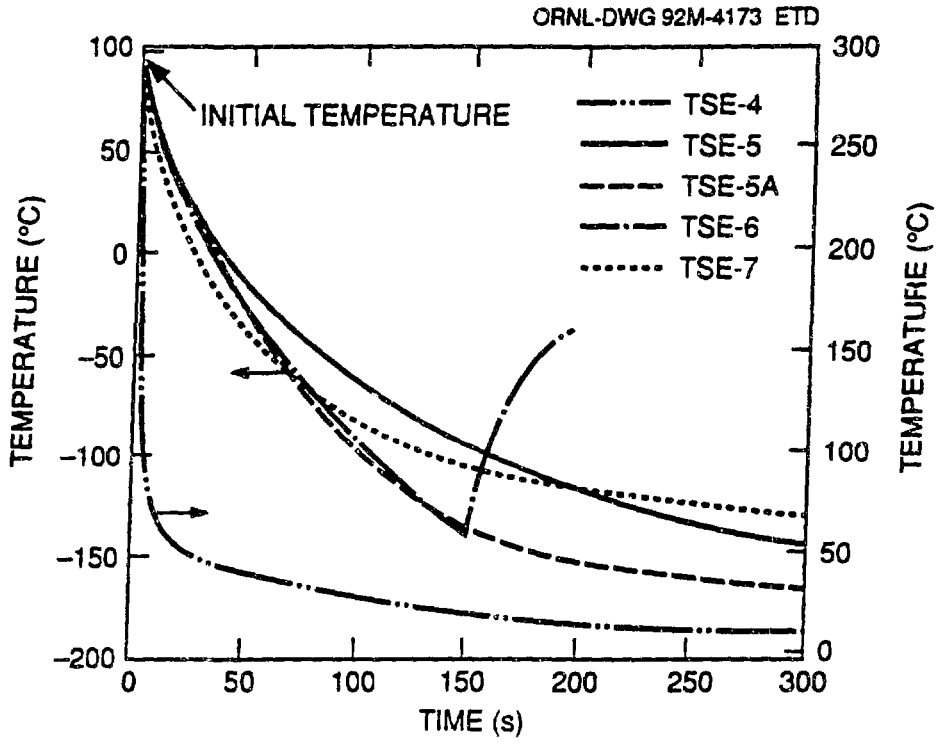

Fig. 8. Inner-surface temperature vs time for TSE-4, 5, 5A, 6, and 7.

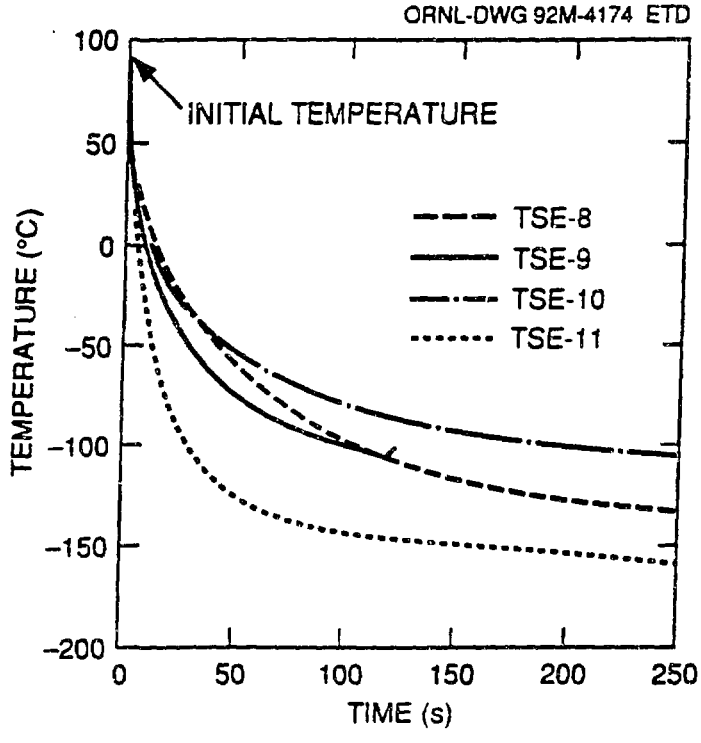

Fig. 9. Inner-surface temperature vs time for TSE-8, 9, 10, and 11.

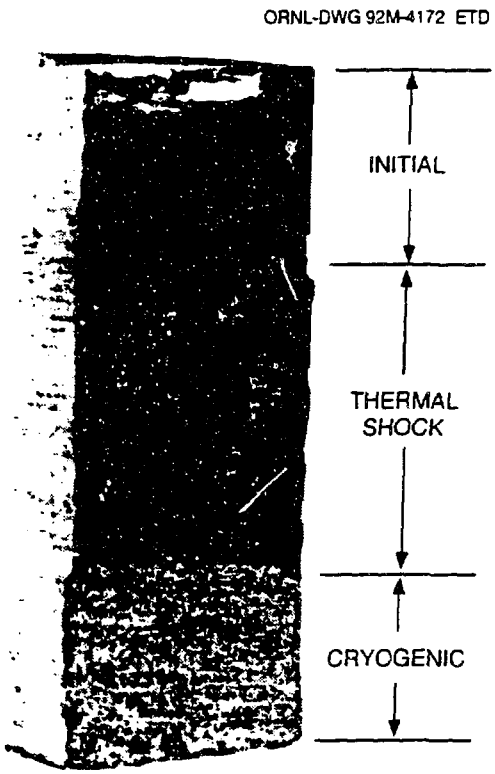

Fig. 10. Fracture surface for TSE-4.

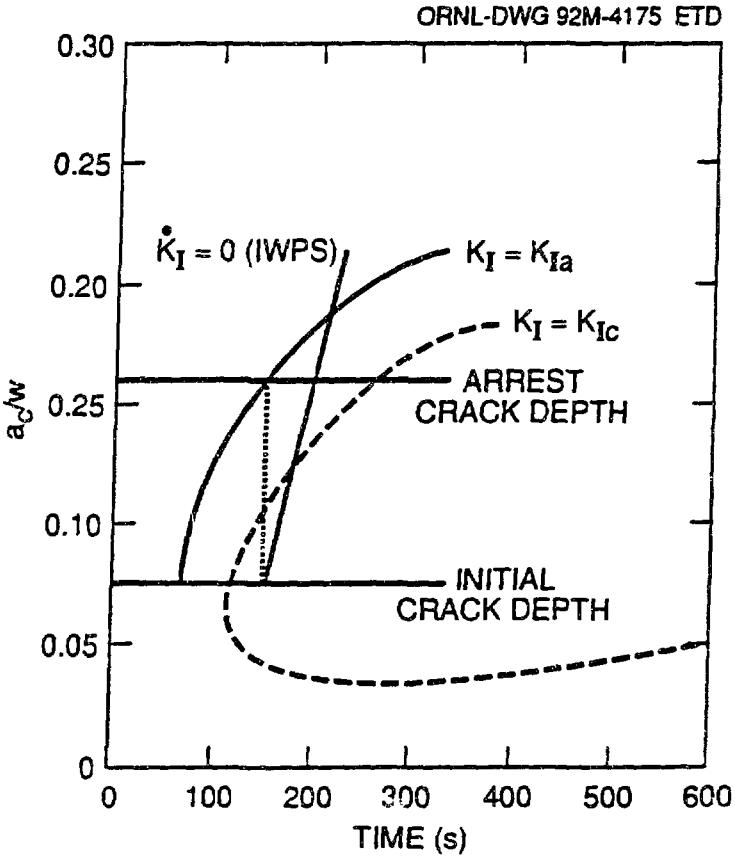

Fig. 11. Critical-crack-depth curves from posttest analysis of TSE-4.

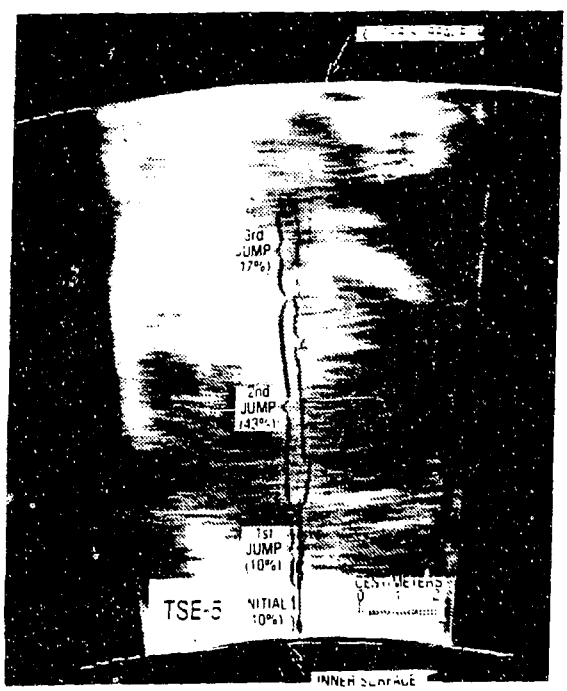

Fig. 12. Fracture profile for TSE-5.

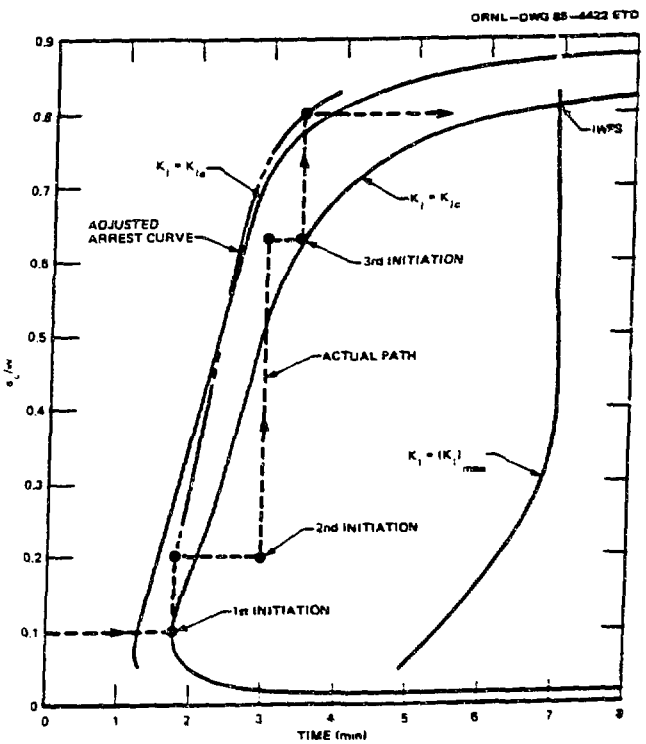

Fig. 13. Critical-crack-depth curves from posttest analysis of TSE-5.

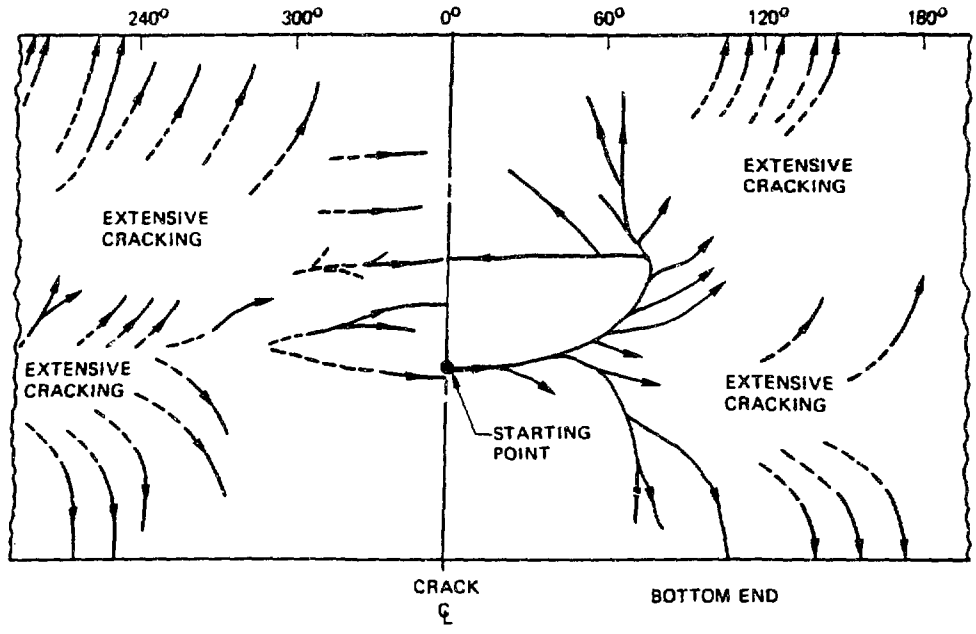

Fig. 14. Developed view of inner surface of TSE-5 test cylinder showing surface extension of initially small (10 mm long × 16 mm deep), circumferential, surface flaw.

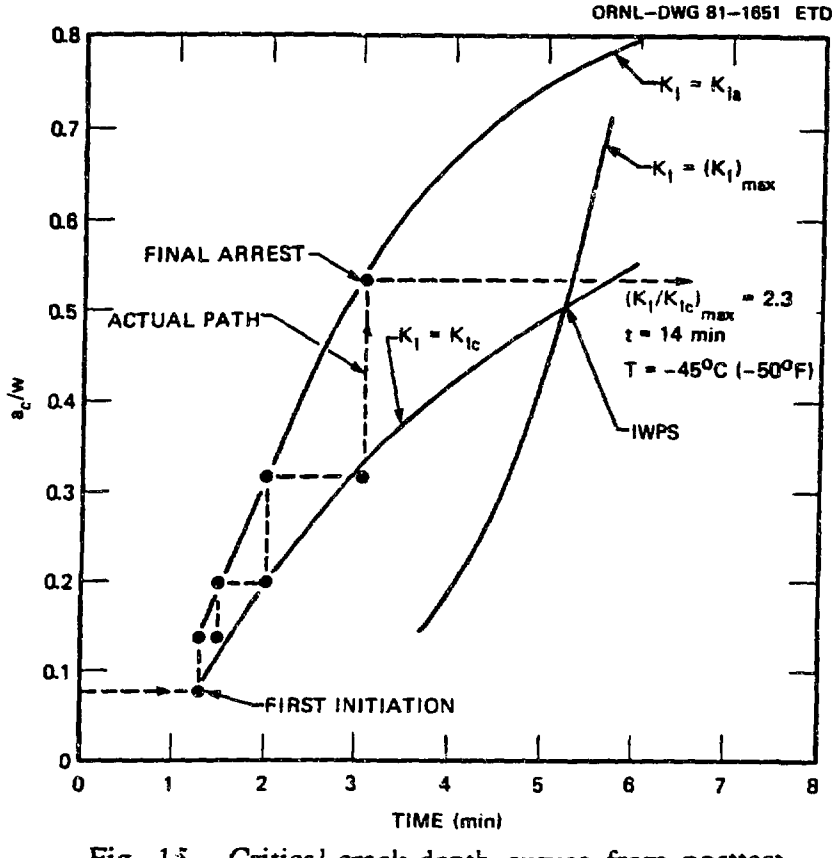

Fig. 15. Critical-crack-depth curves from posttest analysis of TSE-5A.

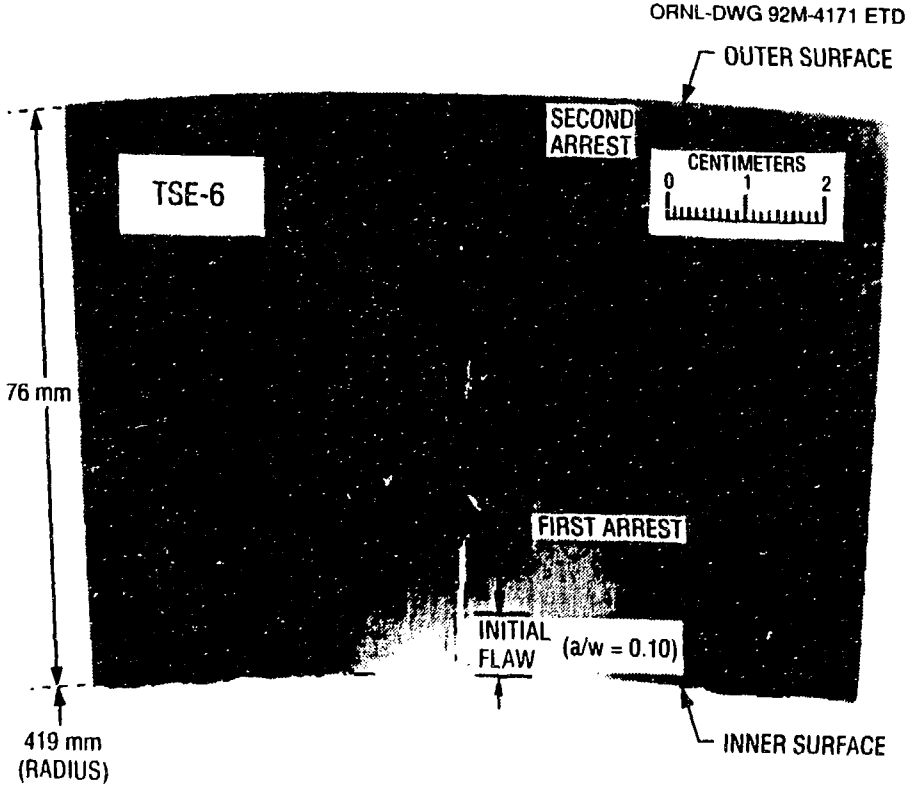

Fig. 16. Fracture profile for TSE-6.

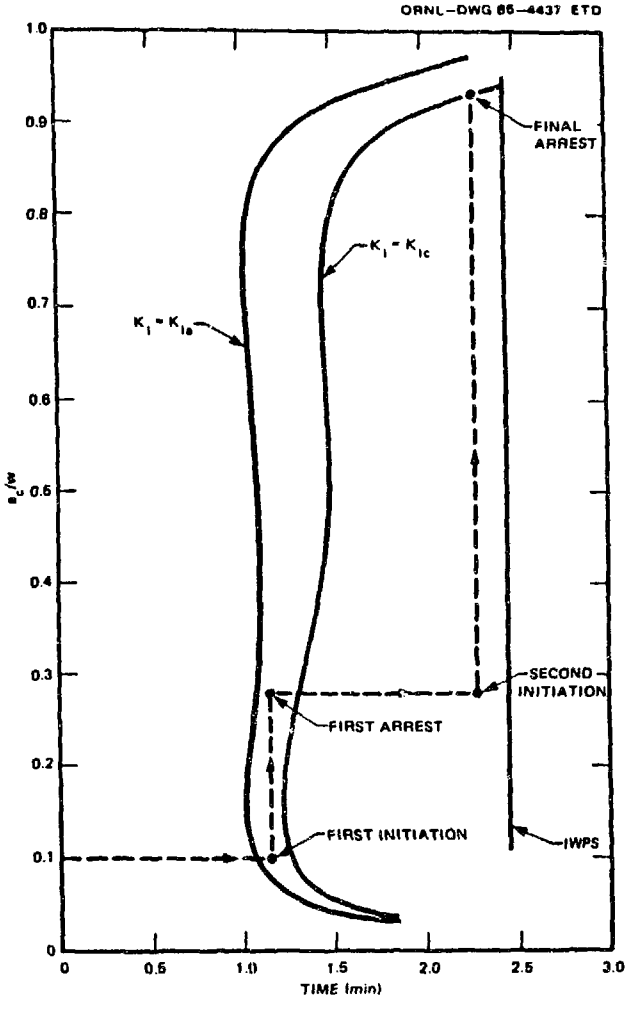

Fig. 17. Critical-crack-depth curves from posttest analysis of TSE-6.

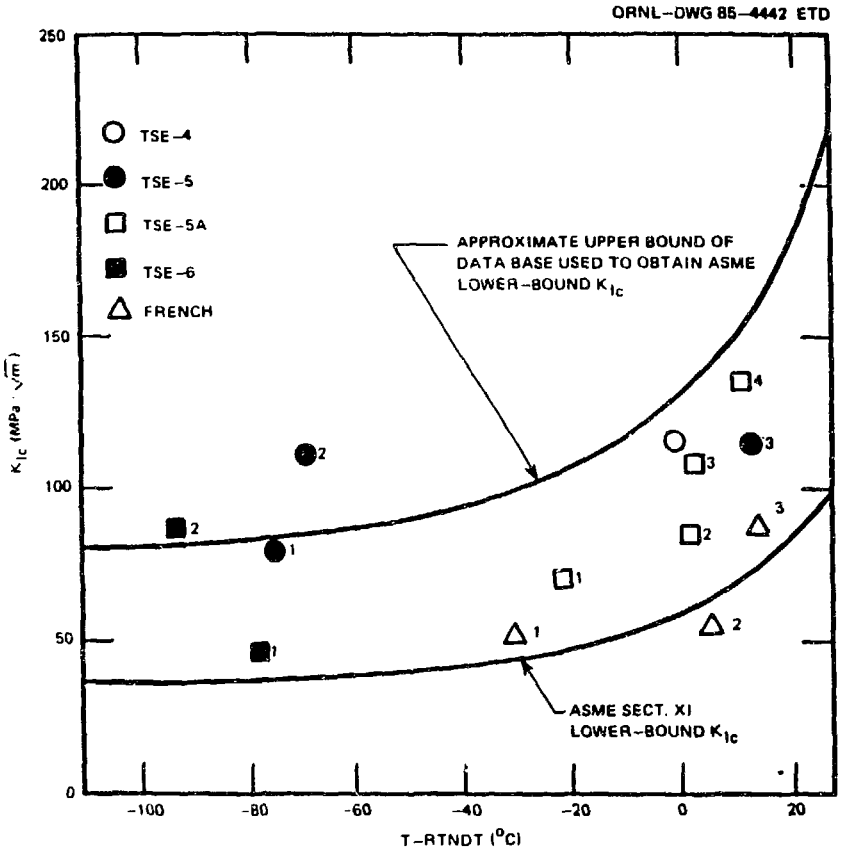

Fig. 18. Comparison of small-specimen and large-specimen K_{Ic} data.

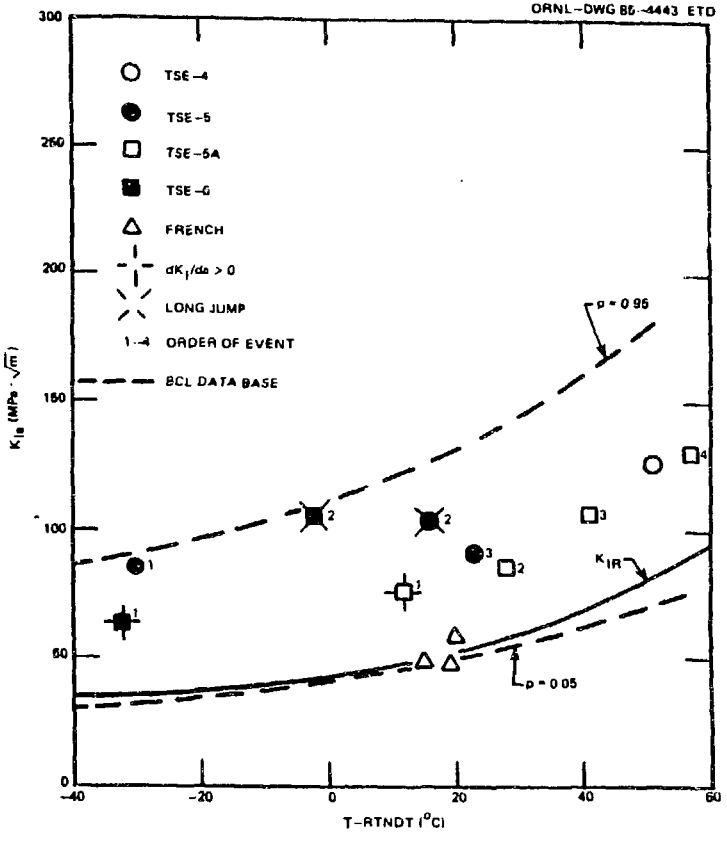

Fig. 19. Comparison of small-specimen and large-specimen K_{Ia} data.

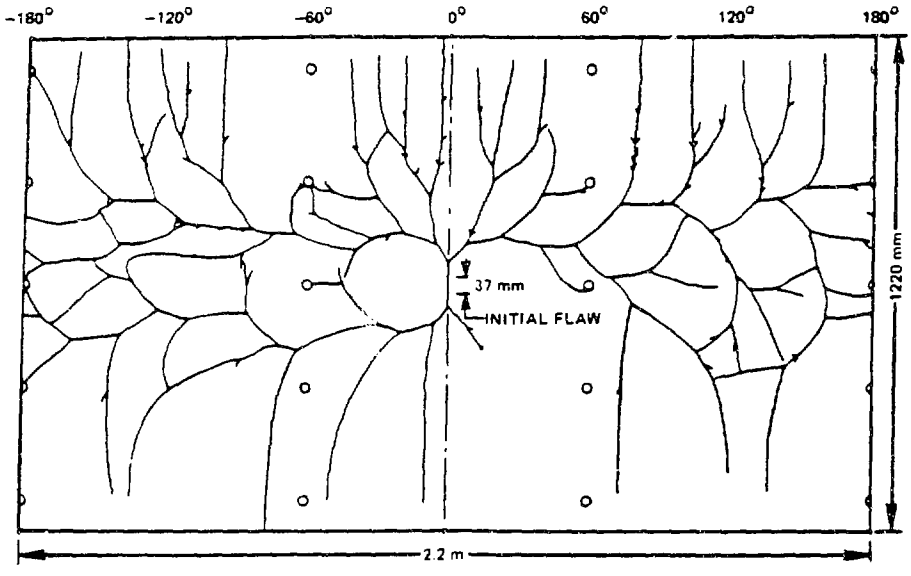

Fig. 20. Developed view of inner surface of TSE-7 test cylinder showing surface extension of initially small flaw (37 mm long × 14 mm deep).

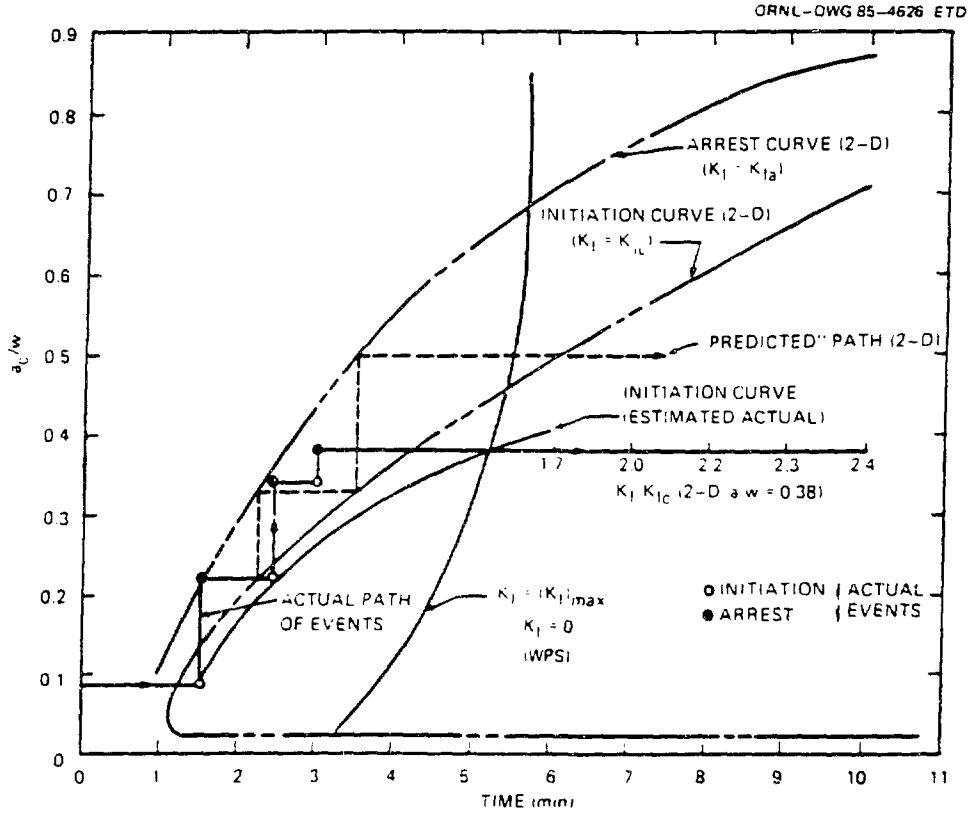

Fig. 21. Critical-crack-depth curves from posttest analysis of TSE-7 (2-D analysis).

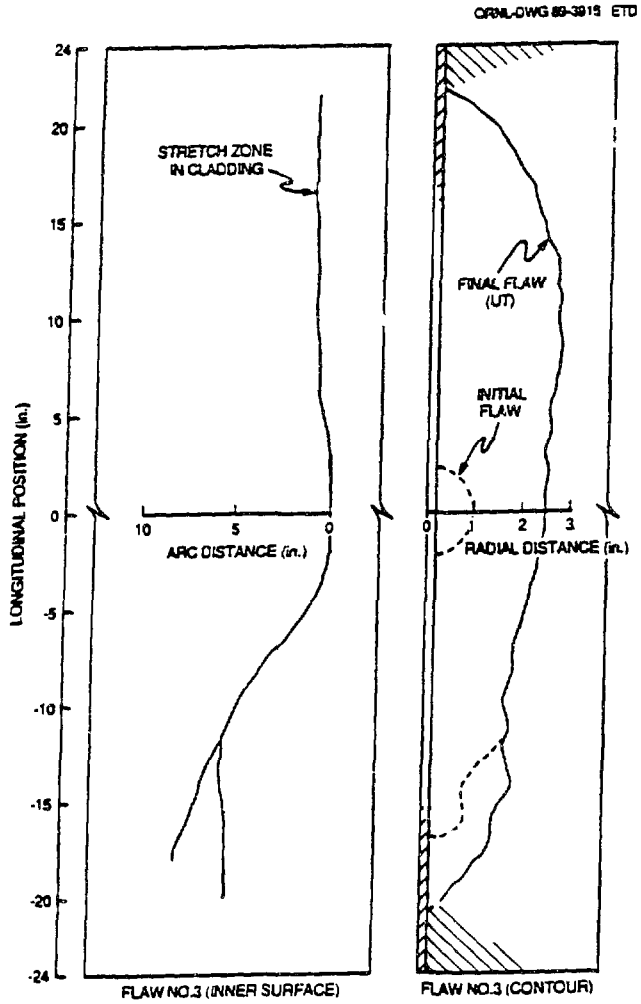

Fig. 22. Stretch-zone and ultrasonic-inspection indications of flaw 3 extension during TSE-8.

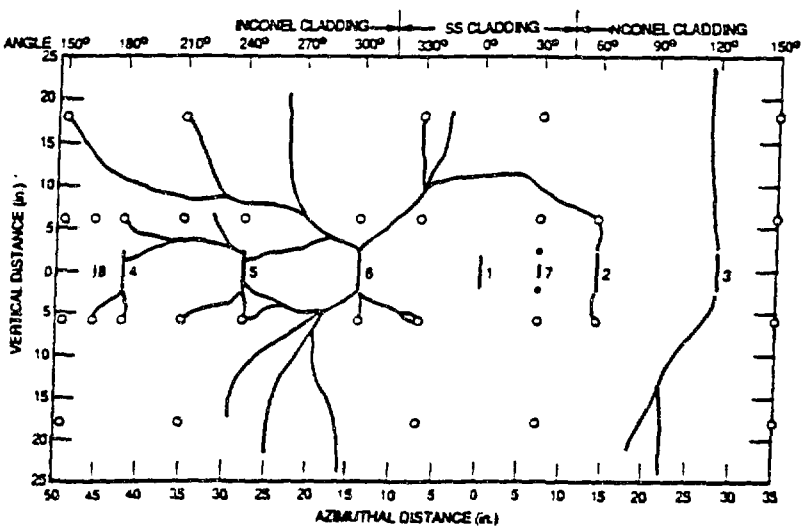

Fig. 23. Developed view of inner surface of test cylinder showing under-clad cracking pattern following TSE-11.